Available online at www.sciencedirect.com
ScienceDirect
International Journal of Heat and Fluid Flow 28 (2007) 341–356
International Journal of HEAT AND FLUID FLOW
www.elsevier.com/locate/ijhff

Influence of hole shape on the performance of a turbine vane endwall film-cooling scheme

W. Colban [a], K. Thole [b,*]

[a] Virginia Polytechnic Institute and State University, Mechanical Engineering Department, 113 Randolph Hall, Blacksburg, VA, United States
[b] Pennsylvania State University, Mechanical and Nuclear Engineering Department, 136 Reber Building, State College, PA, United States

Received 25 February 2006; received in revised form 28 April 2006; accepted 2 May 2006
Available online 7 July 2006

Abstract

Rising combustor exit temperatures in gas turbine engines necessitate active cooling for the downstream turbine section to avoid thermal failure. Film-cooling has long been an integral part of turbine cooling schemes. Cooling the endwall of a turbine airfoil is particularly difficult as much of the coolant is swept off the endwall by vortical flow patterns that develop in the passage. Although film-cooling has potential cooling benefits, this cooling method also leads to increased aerodynamic penalties in terms of total pressures losses in the turbine stage.

This study investigated the trade-off between the cooling benefit and aerodynamic penalties associated with cooling the turbine endwall region for two different cooling hole shapes. Two commonly used film-cooling hole geometries were investigated; cylindrical holes and shaped holes.

Compared to the case without any film-cooling, results showed that film-cooling with either hole geometry increased the aerodynamic losses through the turbine stage. Shaped film-cooling holes generated less total pressure losses through the turbine vane passage than cylindrical holes as a result of the separation from cylindrical hole injection having increased mixing losses. Shaped holes also provided better cooling to the endwall region than cylindrical holes, making them more effective both aerodynamically and thermally.

Keywords: Film-cooling; Turbine cooling; Vane endwall; Aerodynamic losses

1. Introduction

Increasing energy demands require more powerful and more efficient industrial gas turbine engines. One means of achieving this goal is to increase the combustion temperature, resulting in higher temperatures at the inlet of the turbine. Although this is beneficial in terms of power output, it is anything but beneficial in terms of component life. Turbine inlet temperatures are so high in today's gas turbine engines that in the absence of complex cooling schemes the turbine components would completely melt. Ultimately, engine designers aim to accomplish two seemingly opposed tasks; to provide better cooling to the critical surfaces while at the same time minimizing the total amount of coolant used. Coolant comes at a cost to an engine's overall efficiency, as it is bled from one of the compressor stages.

The most common cooling method used for turbine airfoils is that of film-cooling. Film-cooling is a method whereby the coolant is extracted from the compressor stage and then injected through the airfoil surfaces through small holes placed in the surface. While film-cooling significantly helps to cool the part, the reintroduction of this coolant flow into the hot external flow results in an increase in the total pressure loss in a turbine stage. As such, an important consideration for the use of film-cooling is the cooling benefit relative to the aerodynamic penalties that are incurred.

* Corresponding author. Tel.: +1 540 231 7192; fax: +1 540 231 9100.
E-mail addresses: wcolban@sandia.gov (W. Colban), kthole@mne.psu.edu (K. Thole).

0142-727X/$ - see front matter © 2006 Elsevier Inc. All rights reserved.
doi:10.1016/j.ijheatfluidflow.2006.05.002

Nomenclature

C	true vane chord
D	film-cooling hole diameter
I	local momentum flux ratio, $I = \rho_{cool} U_{cool}^2 / \rho_{in} U_{in}^2$
k	thermal conductivity
$\dot{m}$	mass flow rate
M	local blowing ratio, $M = \rho_{cool} U_{cool} / \rho_{in} U_{in}$
P	pressure, vane pitch
PS	pressure side
Re	Reynolds number, $Re = U_{in} C / v$
S	distance along the surface of the vane, measured from the vane stagnation
SS	suction side
t	hole breakout distance
T	temperature
U	velocity
V_n	velocity normal to the streamwise direction, $V_n = V_s \sin(\Psi_{ms} - \Psi)$
V_s	streamwise velocity
V_z	spanwise component of velocity, $V_n = V_s \sin(\Phi)$
X	axial coordinate measured from the vane stagnation
Y	pitchwise coordinate
Y_0	total pressure loss coefficient, $Y_0 = (P_{0,ref} - P_{0,exit}) / (P_{0,ref} - P_{s,exit})$
Z	spanwise coordinate

Greek

α	inclination angle
δ	boundary layer thickness
v	kinematic viscosity
η	adiabatic film-cooling effectiveness, $\eta = (T_\infty - T_{surf}) / (T_\infty - T_{cool})$
ρ	density
ϕ_1	lateral diffusion angle
ϕ_2	forward expansion angle
Φ	pitch angle
Ψ	yaw/flow turning angle

Subscripts

∞	freestream
base	baseline case without any film-cooling
cool	coolant
cyl	cylindrical holes
exit	exit plane
fs	fan-shaped holes
in	inlet condition
max	maximum value
ms	mid-span
no up	no upstream injection
0	total, uncooled effectiveness for conduction correction
plen	plenum
ps	pressure side
ref	reference value
s	static
ss	suction side
surf	surface
up	upstream injection

Overbar

–	lateral/pitchwise average
=	area average or mass average

One region in particularly where high external flow temperatures are detrimental is the endwall platform for the airfoils. This region is particular important when one considers that there are strong vortical patterns that develop, which tend to sweep the film-coolant away from the surfaces and generate much of the aerodynamic losses through a turbine stage. These vortical patterns include a leading edge horseshoe vortex that wraps around either side of the airfoil. The pressure side leg of the horseshoe vortex is then intensified by the cross-passage pressure gradient between adjacent airfoils ultimately forming a much larger passage vortex.

Methods of reducing harmful secondary flows include endwall profiling, upstream injection, and endwall contouring. A reduction in secondary flows resulting from endwall contouring can be achieved through ensuring that the airfoil is more aft-loaded with the minimum static pressure location located further downstream along the airfoil. Another method that has been used to try and diminish the strength of secondary flows is to implement coolant ejection upstream of the first vane row. Coolant ejection re-energizes the boundary layer and reduces the strength of the pressure gradients that lead to the formation of passage secondary flows. Although the main purpose of the high-momentum high-angle upstream injection is to actively control the formation of secondary flows, that injection can also provide some additional cooling benefit.

The purpose of this study was two-fold. The first goal was to compare both the aerodynamic and cooling performances of the two film-cooling hole geometries, cylindrical and shaped film-cooling holes. The second objective was to gain a better understanding of the vortical flow development for these two different cooling hole shapes through flow field measurements.

2. Past studies

Because of the absolute necessity of effective turbine cooling in gas turbine engines, film-cooling has been

researched exhaustively for the last 50 years (Kercher, 2003, 2005). Among the topics studied are hole geometry variations and internal and external conditions such as blowing ratio, density ratio, turbulence level, surface curvature, pressure gradient, cross-flow (internal and external), surface roughness, and hole location. Two comprehensive reviews on the development of film-cooling technology over the years are offered by Goldstein (1971) and Bogard and Thole (2006), with a third more specific review for shaped film-cooling holes by Bunker (2005). In terms of hole location, the endwall region is a particularly difficult region for film-cooling designers, partly because of secondary flows, but also partly because of manufacturing difficulties.

Perhaps the most difficult obstacle facing film-cooling designers in the endwall region is the cross-passage flow. The pressure gradient that develops across the passage from the pressure to suction sides has severe cooling consequences. Coolant is swept away from the near wall region, exposing the endwall surface to hot gas flow. This effect has been documented for upstream slot flow cooling by Blair (1974), Granser and Schulenberg (1990), Friedrichs et al. (1995, 1997), Colban et al. (2003), Knost and Thole (2003, 2005). Other studies, such as those by Harasgama and Burton (1992) and Nicklas (2001), have also verified this effect for endwall film-cooling located in the vane passage.

In addition to the thermal penalties associated with the nozzle guide vane secondary flows, there are also aerodynamic penalties that accompany secondary flows in the form of total pressure losses and non-uniform flow turning. Note that secondary flows are defined as the vortical patterns that develop in the turbine airfoil passages. Langston et al. (1977), in a study performed without endwall blowing, showed a significant loss in total pressure corresponding to the center of the passage vortex as it migrated through the passage. They showed that at the exit plane, the location of the passage vortex and the corresponding loss core had migrated to the suction side of the vane and had risen off of the endwall.

A number of studies, including Sieverding and Wilputte (1981), Friedrichs et al. (1995), Kost and Nicklas (2001), and Barigozzi et al. (2005) have reported aerodynamic benefits associated with endwall film-cooling in the form of reduction of the size and strength of the passage vortex and a reduction in strength of the cross passage flow. However, there is an aerodynamic downside to film-cooling injection, as Friedrichs et al. (1997) reported that film-cooling ultimately increases the total pressure losses through the passage. They showed that the additional losses generated within the hole and the losses generated by coolant mixing with the freestream outweigh the reduction in losses associated with a reduction in secondary flows.

Both passive and active solutions to the problems associated with passage secondary flows are being implemented into nozzle guide vanes. Passive solutions include endwall contouring (Oke et al., 2000) and leading edge fillet designs, such as those presented by Zess and Thole (2002), Lethander and Thole (2003), Becz et al. (2003), and Mahmood et al. (2005). One active solution that is currently employed in some designs is to inject high momentum coolant upstream of the vane passage, in many cases in a double row staggered configuration. Zhang and Jaiswal (2001) measured endwall film-cooling effectiveness on an endwall downstream of two staggered rows of 45° cylindrical holes placed upstream of the vane passage. They showed that at low injection rates the coolant was swept towards the suction side, indicating a strong cross-passage flow. As the injection rate was increased, the cross-passage flow was diminished, and a more complete cooling coverage was seen on the endwall. Using 30° cylindrical holes upstream of a contoured endwall, Zhang and Moon (2003) showed similar results, showing less cross-passage flow at higher injection rates.

A study comparing total pressure losses between an uncooled endwall, a cooled endwall with cylindrical holes, and a cooled endwall with shaped holes was performed by Barigozzi et al. (2005). They reported that there was no significant difference between the secondary flow field with cylindrical holes versus conical diffuser shaped holes. They showed that for low injection rates, the magnitude of the total pressure losses in the loss core of the passage vortex increased relative to the uncooled case. In addition, the location of the center of the passage vortex and its associated loss core shifted positions. For higher injection rates, the passage vortex migrated towards the pressure side and nearly vanished at the highest injection rate, yielding a nearly two-dimensional loss distribution at the exit plane. Barigozzi et al. (2005) reported almost the same performance in terms of film-cooling effectiveness for the two different hole shapes at low mass flow rates, but reported significantly better cooling performance by the shaped holes at high mass flow rates. Note that their study featured different hole patterns in each passage, which meant that it was not a direct one-to-one comparison.

In a parallel study to this paper, Colban et al. (2006a) compared the film-cooling performance of cylindrical holes and fan-shaped holes on a turbine vane endwall. They had the same experimental setup as the current study, with two passages having the same layout, one with cylindrical holes and the other with fan-shaped holes. The study of Colban et al. (2006a) featured upstream injection from two staggered rows of cylindrical holes. The additional contribution of the present study was to give results without upstream coolant injection. Colban et al. (2006a) reported an average augmentation in film-cooling effectiveness of nearly 75% for the fan-shaped passage over the cylindrical passage. The coolant in the fan-shaped passage stayed attached to the surface for the mass flow rates that were tested, while the coolant in the cylindrical passage did not.

The missing element in the research that has been performed is the investigation into the effect of high momentum coolant injection using holes upstream of the vane passage on the downstream endwall film-cooling. The

studies so far have either looked at upstream injection alone, or endwall passage film-cooling alone, but the interaction between the two has heretofore not been investigated. This study presents total pressure losses for two passages – one with cylindrical holes and the other with fan-shaped holes – both with and without upstream coolant injection. All four cases are compared to the solid endwall case with no film-cooling. In addition, film-cooling effectiveness measurements on both endwalls are presented at three different mass flow rates both with and without upstream coolant injection.

3. Experimental facilities

All experiments were performed in the low-speed, large scale, recirculating wind tunnel facility shown in Fig. 1. The flow was split into three separate channels, with the center channel being heated to represent the combustor core flow using a 55 kW bank of strip heaters. The lower channel was blocked for this study, while the upper channel was cooled using a 44 kW chiller and used to provide film-cooling for the endwall in the vane cascade test section. The temperature difference between the heated mainstream and the film coolant that was achieved for the heated flow adiabatic effectiveness tests was on the order of 20 °C. The flow field measurements were unheated, with both the coolant and the mainstream at the same temperature.

The relevant inlet conditions for the tests are listed in Table 1, along with important geometric parameters. An engine representative inlet Reynolds number of 3.4×10^5 based on the true vane chord and the inlet velocity was maintained for all tests. The nozzle guide vanes were scaled up by a factor of three from the engine. Inlet velocity and total pressure profiles where taken at several pitch locations a distance of one chord length upstream of the vane stagnation to ensure periodic inlet conditions and also to measure the reference mass-averaged total pressure used in the total pressure loss calculations. The mass averaged inlet velocity was 9.4 m/s for all experiments. From the velocity profile measurements, the boundary layer at one chord length upstream of the vane leading edge was determined to be 27% of the vane span. A hot wire anemometer was used to measure the turbulence intensity at a distance of one chord length upstream of the vane leading edge. The turbulence intensity was measured at several span and pitch locations and was found to be a uniform value of 1.2%. The heated tests were nominally incompressible, with a coolant-to-mainstream density of nearly 1.06.

Table 1
Operating conditions and vane parameters

Scale	3X
C (m)	0.53
$S_{max,PS}$ (m)	0.52
$S_{max,SS}$ (m)	0.68
U_{in} (m/s)	9.41
Re_{in} (–)	3.4×10^5
ΔT (°C)	20
P (m)	0.465

In the gas turbine community, aerodynamic penalties are typically discussed in terms of total pressure loss through the turbine cascade. The total pressure loss is typically referenced to the mass averaged value upstream of the turbine inlet. Similarly, the cooling performance of a given film-cooling design is typically reported in terms of adiabatic film-cooling effectiveness, which is essentially the temperature of the fluid just above the critical surface. Adiabatic film-cooling effectiveness accurately describes the behavior of the coolant on the surface.

3.1. Test section design

The test section, described in detail by Colban et al. (2006a), was a two-passage linear vane cascade with one contoured endwall and one flat endwall. The upper endwall was contoured in order to match the non-dimensional static pressure distribution at low speed test conditions to that found in the engine at high speed operating conditions. This was important because the static pressure distribution around the vane has a strong influence on the development

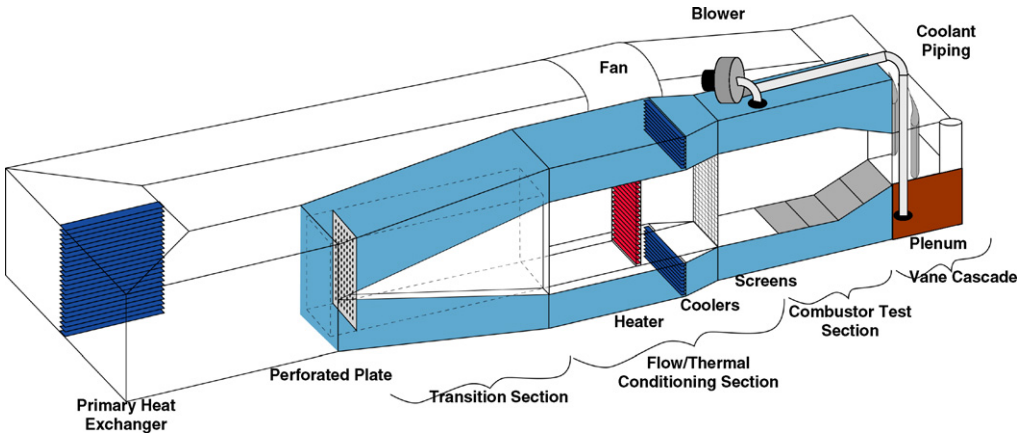

Fig. 1. Diagram of the large-scale, low-speed, recirculating wind tunnel facility.

of secondary flows through the vane passage, both on the strength and location. The development and design of the contoured endwall was also documented by Colban et al. (2006b) and featured a 40% contraction of the span from the leading edge to the trailing edge. Both experimental results (Colban et al., 2006b) and computational predictions (Colban et al., 2005) of the passage flow field show a nearly two-dimensional pressure distribution below 40% of the inlet span height.

The vane cascade featured two periodic passages, each with an identical film-cooling hole pattern, but with a different film-cooling hole geometry. The film-cooling hole layout is shown in Fig. 2, with a callout and details of each cooling hole shape. The specific geometric parameters for each cooling hole shape are given in Table 2. The diameter of all the holes (including the entrance length for the fan-shaped holes) was 2.6 ± 0.15 mm. The double rows of upstream holes were oriented in a staggered array. The surface angle of the upstream holes was 60° from horizontal and each hole had an orientation angle that was directed towards the center of the passage. All of the holes in the passage had a shallower surface angle of 35° and were angled nominally in the direction of the inviscid streamline at that location. The holes in the fan-shaped passage also featured a lateral diffusion angle of 10° and a forward diffusion angle of 10°.

A single plenum, which provided coolant to supply the entire endwall, was located beneath the test section. The capability was available to block off each passage individually, as well as the rows of upstream holes, and measure exactly the amount of coolant mass flow delivered to the entire endwall using a laminar flow element. The amount of coolant in this study was reported in terms of percent difference from the baseline case, which was chosen to reflect typical coolant flow rates in the first stage of an industrial gas turbine.

Table 2
Film-cooling hole parameters

	Upstream	Cylindrical	Shaped
α (deg)	60	35	35
ϕ_1 (deg)	0	0	10
ϕ_2 (deg)	0	0	10

The endwall was constructed from a medium density foam material using a five-axis water jet for high geometrical integrity of the hole design and pattern. The foam had a low thermal conductivity ($k = 0.028$ W/m K) such that the conduction losses laterally throughout the foam as well as from the surface into the plenum were minimal. A manufacturing fillet was also implemented, circumnavigating the vane at the vane/endwall junction. The fillet was an elliptical design and extended a distance 12D up the vane span and 10D normal to the vane.

3.2. Measurement techniques and data analysis

A five-hole total pressure probe with a 2.4 mm tip was used to measure all three components of velocity and the total pressure at the exit plane. The exit plane is shown schematically in Fig. 2, and it extends from one trailing edge to the other and covers the entire pitch at the exit. The five-hole probe measured streamwise velocity, yaw angle, pitch angle, and total pressure directly.

In order to get an accurate view of the secondary flow vectors in the exit plane, the components were transformed into the coordinates shown in Fig. 2. The streamwise velocity, V_s, was measured directly with the five-hole probe. The horizontal velocity component, V_n, in the exit plane was calculated normal to the streamline at the midspan according to Eq. (1),

$$V_n = V_s \sin(\Psi_{ms} - \Psi) \tag{1}$$

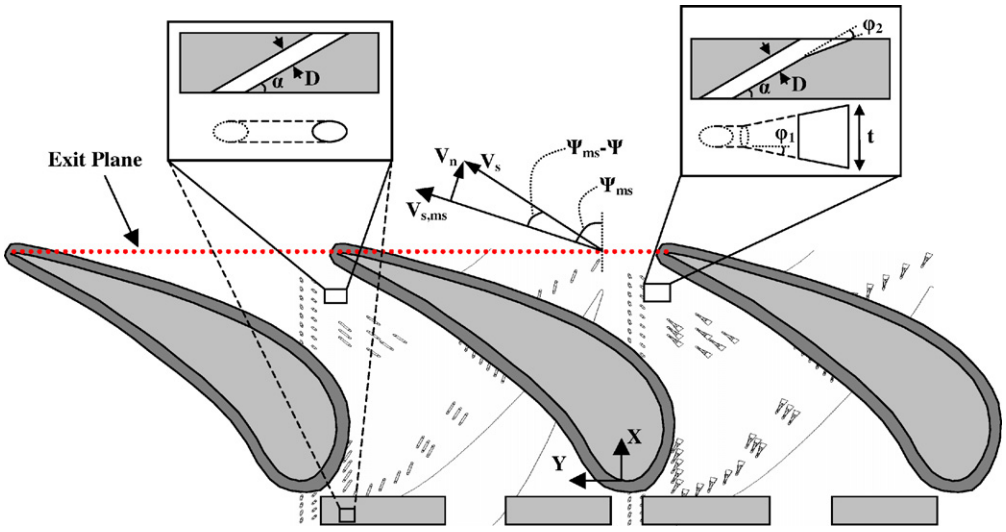

Fig. 2. Film-cooling hole layout and specifications. Upstream injection holes are highlighted as well as the exit plane, which stretches from trailing edge to trailing edge.

where $(\Psi_{ms} - \Psi)$ is the deviation in flow turning angle from the midspan. The vertical velocity component, V_z, in the exit plane was calculated using the measured pitch angle, Φ, according to Eq. (2),

$$V_z = V_s \sin(\Phi) \tag{2}$$

Approximately 240 locations in the exit plane were taken for each of the five cases presented in this study, with higher resolution in areas with larger gradients. At each location, 4 s of data was taken at a sampling frequency of 1000 Hz. The measurement was repeated five times and then averaged, resulting in 20,000 data points for each reported value.

Total pressure loss coefficients were calculated according to the method laid out by Friedrichs et al. (1997), where the total pressure loss coefficient given by Eq. (3),

$$Y_0 = \frac{P_{0,ref} - P_{0,exit}}{P_{0,ref} - P_{s,exit}} \tag{3}$$

where $P_{0,exit}$ and $P_{s,exit}$ were the total and static pressures at the exit. $P_{0,ref}$ was calculated using two different methods. The first way of calculating $P_{0,ref}$ incorporates the additional total pressure and energy added to the passage flow as a result of the addition of film-coolant. The mass-averaged calculation of $P_{0,ref}$ is given by Eq. (4),

$$P_{0,ref} = \frac{P_{0,in}\dot{m}_{in} + P_{0,cool}\dot{m}_{cool}}{\dot{m}_{in} + \dot{m}_{cool}} \tag{4}$$

The second definition used for $P_{0,ref}$ in Eq. (4) was just to set $P_{0,ref} = P_{0,in}$, the mass-averaged inlet stagnation pressure. This definition was used for the uncooled case, in which case Eq. (4) simplifies to that result, and was also calculated for the other flowfield cases. The second definition neglects the total pressure additions from the film-cooling flow, and can be misleading for that reason because it typically yields lower Y_0 values than by using the definition for $P_{0,ref}$ in Eq. (4).

Mass-averaged values of the total pressure loss coefficients were also computed in the exit plane in order to give an overall comparison of each case in terms of complete total pressure loss. The mass-averaging was done according to Eq. (5),

$$\overline{\overline{Y}}_0 = \frac{\int_Z \int_Y Y_0 V_s \rho \mathrm{d}Y \mathrm{d}Z}{\int_Z \int_Y V_s \rho \mathrm{d}Y \mathrm{d}Z} \tag{5}$$

although the density term cancelled out of Eq. (5) because the tests were incompressible, being unheated and at low speed.

Endwall surface temperatures were measured using an infrared camera and converted to adiabatic film-cooling effectiveness. Adiabatic film-cooling effectiveness was a non-dimensionalized temperature, given in Eq. (6),

$$\eta = \frac{(T_\infty - T_{surf})}{(T_\infty - T_{cool})} \tag{6}$$

where T_∞ was the freestream air temperature, T_{cool} was the temperature of the injected coolant, and T_{surf} was the measured surface temperature. Eight image locations were necessary to map the entire endwall surface for each passage. Five images were taken and averaged at each location. A FLIR P20 infrared camera was used with an image resolution of 240×320 pixels, which gave an image resolution of approximately 0.28D per pixel. Each image was calibrated using thermocouples embedded flush with the endwall surface, and then corrected for conduction losses. A one-dimensional conduction correction was applied to the measured film-cooling effectiveness to give the reported adiabatic film-cooling effectiveness. The uncooled effectiveness, η_0, varied between 0.06 and 0.15, and depended on the location on the endwall.

3.3. Experimental uncertainty

Uncertainty estimates were made using the technique described by Moffat (1988), which is a partial derivative and sequential perturbation method. The exit total pressures were measured with a pressure transducer that had a bias uncertainty of ±0.019% of full scale. At the exit plane the precision error was found by averaging 20 independent samples with each sample representing over 10,000 measurements over 90 s. The inlet total pressures were measured with a transducer having a bias uncertainty of ±0.079% of the full scale. The precision uncertainty at the inlet was measured by taking the standard deviation of 25 samples with each sample representing an average of 10,000 measurements over 90 s. The bias, precision, and total uncertainties of all the measured values were used to ultimately calculate Y_0. For a value of $Y_0 = 0.15$ measured in the cylindrical passage with upstream cooling, the uncertainty was calculated to be ±0.001.

The uncertainty in adiabatic film-cooling effectiveness was also calculated for high and low reported values. The bias error associated with type E thermocouples was taken as ±0.2 K, which was the value listed by the manufacturer. The precision uncertainty for the freestream and coolant thermocouples was determined by taking a reading every 10 s while the images were being taken. The standard deviation of those readings, during an assumed steady state for the test section, was taken as the precision uncertainty. The precision uncertainty for the freestream temperature was ±0.25 K, while the precision uncertainty in the coolant temperature measurements was ±0.03 K. The surface temperatures were measured with an infrared (IR) camera. The temperature recorded by the IR camera was calibrated to readings taken by type E thermocouples mounted flush with the measurement surface. Because the IR images were forced onto the measured thermocouple temperatures, one can assume that the bias error for the IR data was the root-sum-square of the thermocouple bias (±0.2 K) and the average difference between the calibrated IR data and the thermocouple measurement (±0.12 K). In this way, the bias error for the surface temperature measurements was ±0.23 K. The precision error for the IR surface temperature measurements was found by taking the standard

Table 3
Test matrix (italicised values indicate exit plane flow field cases, and upstream injection flow rates shown in parentheses)

	Cylindrical passage			Fan-shaped passage		
Upstream	75% (75%)	*100% (100%)*	125% (125%)	75% (75%)	*100% (100%)*	125% (125%)
No Upstream	75% (0%)	*100% (0%)*	125% (0%)	75% (0%)	*100% (0%)*	125% (0%)

deviation of the same points in 10 images taken at steady state at the same location. From this method, the precision error for the IR surface temperature measurements was found to be ±0.27 K, which make the total uncertainty for the IR surface temperature measurements ±0.35 K. For a high value of $\eta = 0.9$, the uncertainty was ±0.012, while a lower value of $\eta = 0.2$ had an uncertainty of ±0.011.

3.4. Test design

The test matrix is shown in Table 3 and includes a total of 13 cases (baseline case with no blowing is not shown). The cases that represent the baseline flow rates for an actual engine are highlighted in Table 3. Note that actual flowrates are not shown for proprietary reasons. Adiabatic film-cooling effectiveness measurements were made for all cases shown in Table 3. Flow field measurements were taken at the exit plane for the highlighted baseline cases in the test matrix. One other case was measured for the exit plane, and that was a case with no blowing, which was meant to be a baseline case for the flow field measurements. The percentages shown in parentheses in Table 3 represent the flow rate from the upstream rows of holes (as shown in Fig. 2).

The flow rates for the six cases without upstream injection were determined by matching the pressure ratio between the endwall plenum total pressure and the vane stagnation total pressure to the corresponding cases with upstream injection. In this way, the passage endwall film-cooling holes had nominally the same flow rates in both the upstream and no upstream blowing cases.

Local inviscid blowing and momentum flux ratios were computed for each hole. The local inviscid velocity was used in the scaling, and the static pressure distribution on the endwall was approximated using a 3D CFD prediction without film-cooling in FLUENT 6.1.2. The experimental total pressure measured in the plenum was then used to predict the inviscid coolant velocity in the metering area of the cooling holes. Local freestream velocities on the endwall were also calculated using the CFD static pressure distribution, and the mainstream and coolant densities were measured during testing. The results are shown in terms of a contour map in Fig. 3(a) and (b). One could also think of Fig. 3(a) and (b) as design maps with which to predict the blowing ratio and momentum ratio for a hole placed at a given location on the endwall. The highest blowing ratios were near the vane stagnation and resulted from the relatively low local velocity at that location. The lowest blowing ratios occurred in the vane passage at the throat region, where local velocities were highest.

4. Aerodynamic results

The streamwise velocity distribution was nearly the same for all five cases except near the wall, so it is shown in Fig. 4 only for the uncooled case. The strong downward velocity near the exit midspan was a result of the upper contoured endwall contraction. Both the streamwise velocity and the secondary flow vectors have been non-dimensionalized by the mass-averaged inlet velocity to the cascade. Fig. 4 shows that the streamwise velocity is nearly two-dimensional across most of the exit plane. There was a local minimum non-uniformity in streamwise

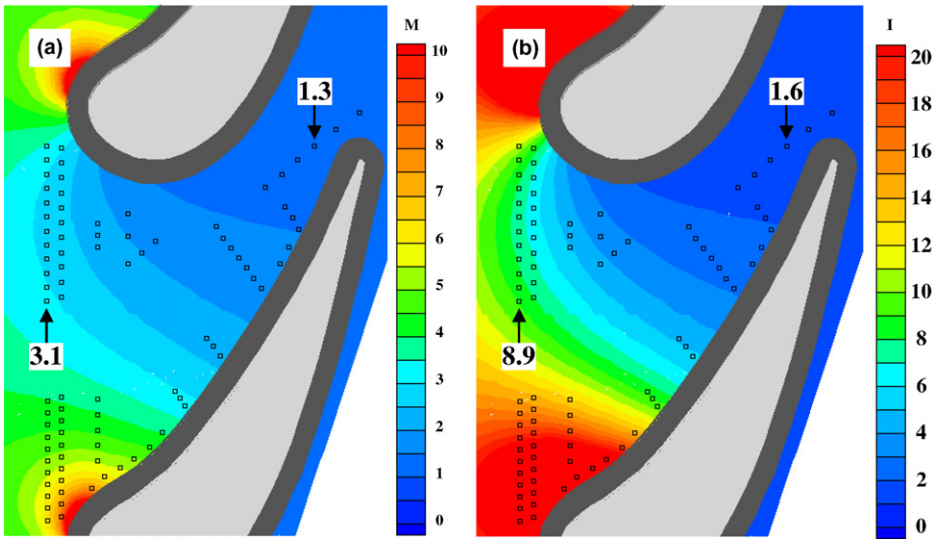

Fig. 3. Contours of calculated (a) blowing ratio and (b) momentum flux ratio for baseline conditions.

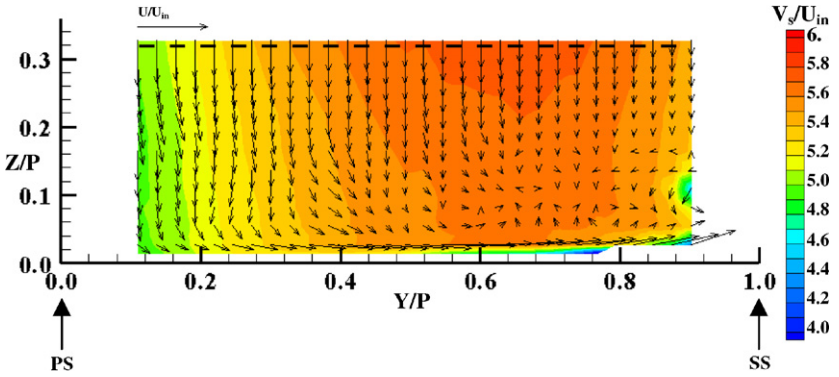

Fig. 4. Contour of streamwise velocity in the exit plane for the uncooled case with superimposed secondary flow vectors.

velocity corresponding to the location of the center of the passage vortex near the suction side at $Y/P = 0.9$ and $Z/P = 0.1$. A strong cross passage flow was seen near the wall from the pressure to the suction sides.

4.1. Total pressure loss measurements

Normalized total pressure losses are shown in Fig. 5(a)–(e). For the baseline uncooled case, the reference total pressure in Eq. (3) was taken as the mass-averaged inlet total pressure, while for the other cases, the reference total pressure was mass-averaged including the coolant flow to incorporate the losses due to film-cooling addition. Upon examining the uncooled case in Fig. 5(a), the most noticeable feature was the loss core associated with the passage vortex, located at $Y/P = 0.9$ and $Z/P = 0.1$. The passage vortex was the most dominant loss generator in the uncooled passage. As mentioned previously, the implemen-

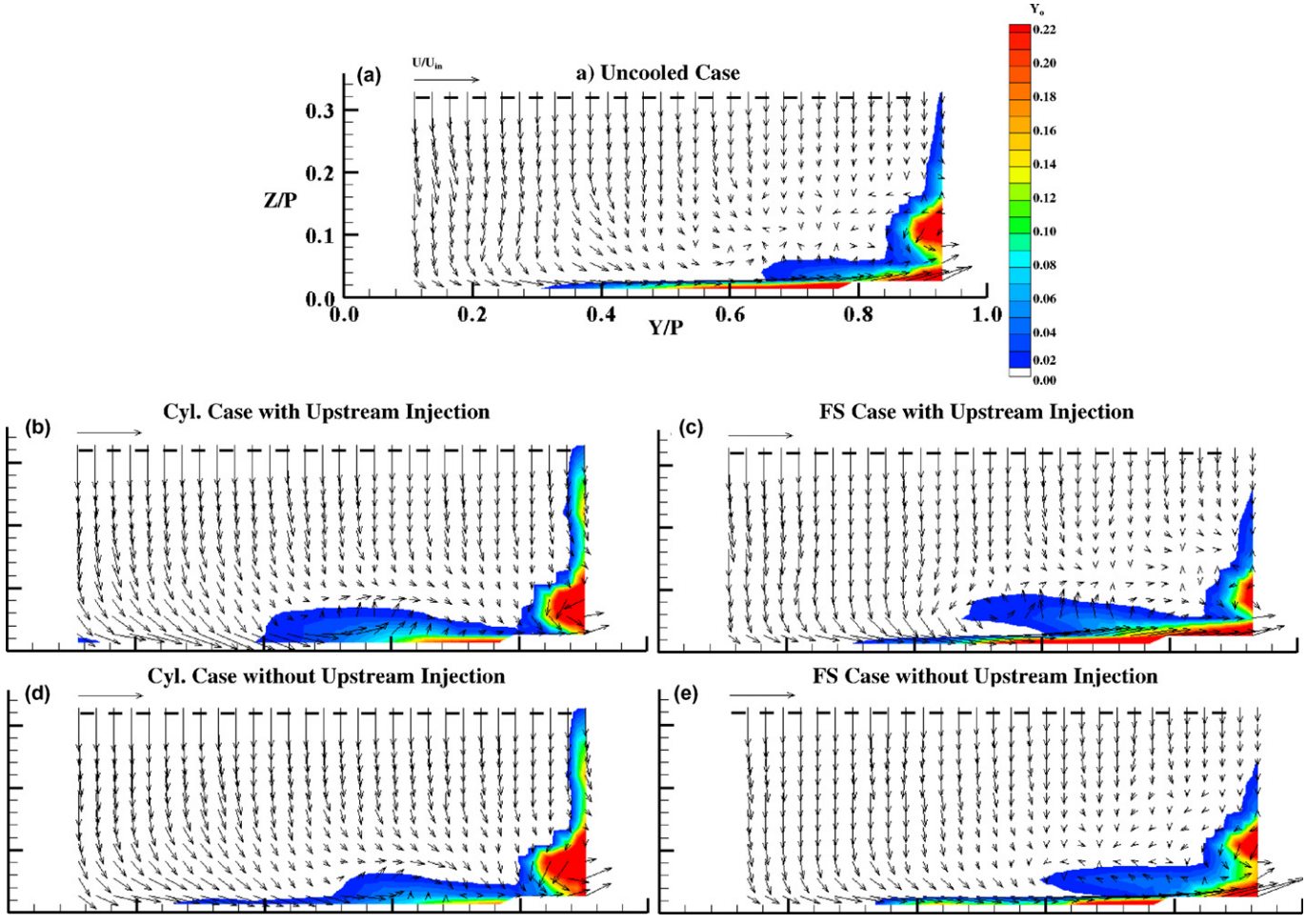

Fig. 5. Contours of total pressure loss measured at the exit plane.

tation of a contoured endwall, which in the present study was used to match the engine airfoil flow distribution, has been shown to suppress the size and strength of passage vortex. This phenomenon was verified by the current study, which showed the size and strength of the passage vortex was smaller than the commonly accepted secondary flow model proposed by Langstion (1980).

As with the streamwise velocity shown in Fig. 4, the secondary flow vectors are superimposed onto the total pressure loss contours in Fig. 5(a)–(e). There was also a region of high losses near the endwall at the suction side corner. Langston et al. (1977) noticed the same phenomenon for an uncooled endwall and attributed it to the separation of the endwall boundary layer.

Fig. 5(b) shows the total pressure losses in the exit plane for the cylindrical passage with upstream injection. Two major changes occurred from the uncooled case. First, the location of the passage vortex shifted away from the suction side, perhaps due to a reduction in strength of the cross passage flow. Secondly, there was a region of high total pressure loss near the endwall wall extending from $Y/P = 0.4$ to $Y/P = 0.7$. These losses were undoubtedly a result of film-cooling jets mixing with the freestream. It is interesting to note that the secondary flow vectors along the wall near $Y/P = 0.5$ appear to be cutting under the mixed out film-cooling region and lifting it away from the surface.

The total pressure loss contour and secondary flow vectors for the cylindrical passage without upstream injection are shown in Fig. 5(c). The same general trends as for the case with upstream injection were seen, including the change in location of the passage vortex and the high losses near the wall from jet/freestream mixing. The main difference was that the mixing losses near the wall were not as great for the case without upstream injection. This suggests that the region of high mixing losses near the wall was partly caused by the upstream injection, in addition to the passage film-cooling.

Total pressure losses for the fan-shaped passage are shown in Fig. 5(d) (upstream injection) and Fig. 5(e) (no upstream injection). For the case with upstream coolant injection, the position of the passage vortex remained unchanged from the uncooled case. The total pressure losses generated near the endwall for the fan-shaped passage had a strikingly different pattern than for the cylindrical passage. In the region from $Y/P = 0.5$ to $Y/P = 0.75$, the losses near the endwall in the fan-shaped passage decreased with span up to a height of approximately $Z/P = 0.04$. At that height, the losses increased again and showed a relative maximum at $Z/P = 0.06$. This pattern suggests that the film-cooling flow stays attached to the surface, with less loss in that region. The losses centered at $Z/P = 0.06$ would then be caused by the shear between the coolant layer and the freestream. Again, as with the cylindrical passage, some of the near wall losses appear to be a result of upstream injection, as they were greater for the case with upstream injection. The secondary flow vectors in the fan-shaped passage, although they indicated a stronger cross flow, did not seem to show the lift-off of near wall flow as with the cylindrical passage.

It is also useful to examine the change in total pressure losses that result from the addition of film-cooling. Fig. 6(a)–(d) shows the change in total pressure loss coefficient from the uncooled case to each film-cooled case. Note that a negative value of $(Y_0 - Y_{0,\text{base}})$ indicated a decrease in total pressure relative to the uncooled case, while a positive value of $(Y_0 - Y_{0,\text{base}})$ meant there was an increase in total pressure. For all film-cooled cases, the majority of the passage shows virtually no change in total pressure loss from the uncooled case. Both cylindrical hole cases showed a large increase in total pressure in the region of the passage vortex. The increase was partially attributable to the

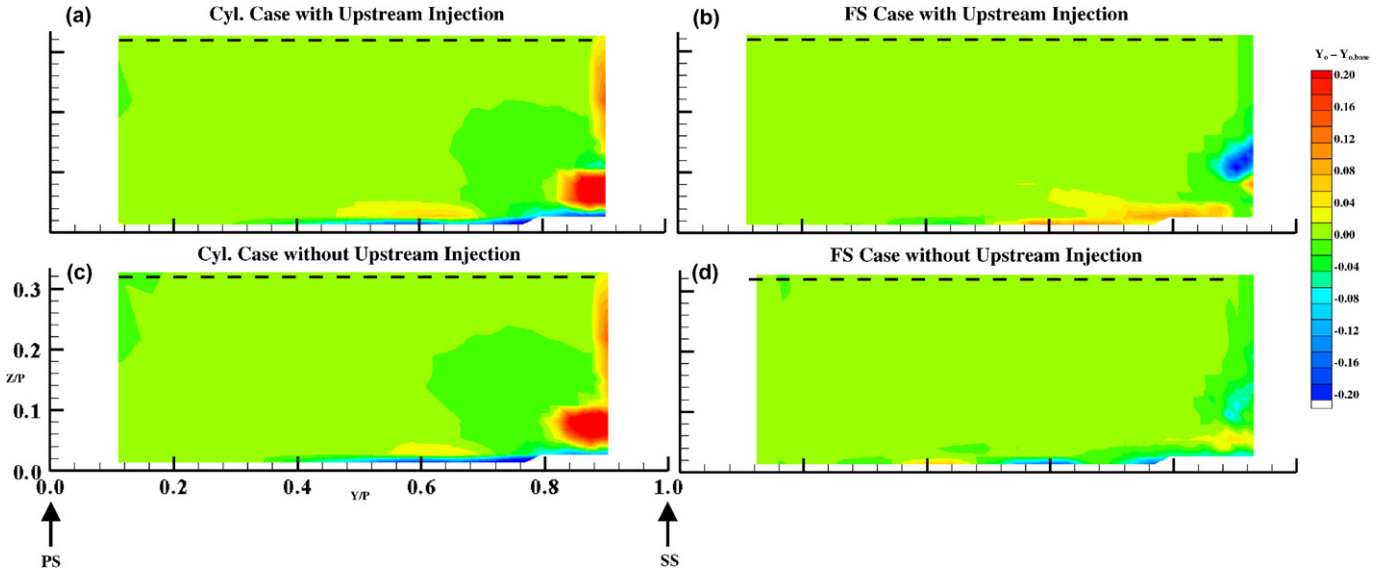

Fig. 6. Contours of change in total pressure loss coefficient from the uncooled case measured at the exit plane.

shift in location of the loss core away from the suction surface for the two cylindrical cases. However, it is likely that the maximum loss associated with the passage vortex was also enhanced. Barigozzi et al. (2005) also reported an increase in total pressure loss generated by the passage vortex for a similar flow rates with cylindrical hole film-cooling relative to the uncooled case.

For the fan-shaped passage, $(Y_0 - Y_{0,\text{base}})$ values increased for the upstream injection case in the shear layer mixing region, as shown in Fig. 6(c). However, the upstream injection seemed to reduce the losses associated with the passage vortex for the fan-shaped case. The fan-shaped case without upstream cooling was the most similar to the uncooled case in terms of total pressure loss. There was very little change in either magnitude or distribution of the total pressure losses from the uncooled case to the fan-shaped case without upstream injection, with only a slight reduction in losses associated with the passage vortex and a slight increase in losses because of mixing and shear within the passage.

Because the main purpose of the nozzle guide vanes is to turn the flow as it enters the downstream first blade row, which extracts energy from the expanding hot gases, the exit angle of the flow through the passage is extremely important. Secondary flows such as the near wall cross flow decrease the overall efficiency of the engine because they alter the exit flow angles. Engine designers would like to have as uniform an exit flow angle as possible, or else the blade design must include these flow angles. Fig. 7 shows pitch-averaged flow angles at the exit plane for each of the five cases as the difference from the midspan flow turning angle. The uncooled case had very little variation above $Z/Z_{\max} = 0.1$. Both fan-shaped cases had a similar distribution of flow-turning angles along the span, with slightly higher turning near the wall. The cylindrical cases had significantly less turning in the near wall region, which means that the endwall cross flow was reduced. This corresponds to the shift in location of the passage vortex towards the pressure side from the uncooled case (Fig. 5(a)–(c)). Although the cylindrical passage cases had less endwall cross flow, they did have a higher flow turning angle than the uncooled case from $Z/Z_{\max} = 0.1$ to $Z/Z_{\max} = 0.25$. The difference in flow turning angles between the uncooled cases and the cases with film-cooling stresses the importance of incorporating the changes in flowfield that are brought upon by film injection into the aerodynamic portion of the airfoil design.

4.2. Mass-averaged total pressure loss

Total pressure losses were mass-averaged according to Eq. (3) using the two different definitions of $P_{0,\text{ref}}$, and those values are shown in Fig. 8 for each flow case. The most obvious conclusion from the mass-averaged total pressure losses in Fig. 8 is that cylindrical film-cooling greatly increased the total pressure losses through the vane passage, both with and without upstream blowing. Friedrichs et al. (1997) also noted an increase in overall total pressure loss through the turbine cascade for cylindrical hole cooling. The results from this study verify the findings of Friedrichs et al. (1997) for cylindrical holes, but suggest something different for fan-shaped holes. The mass-averaged total pressure losses through the turbine cascade for fan-shaped holes were only slightly higher than the uncooled case for the case without upstream injection. Even the fan-shaped case with upstream injection had a lower mass-averaged total pressure loss than the cylindrical case without upstream injection. The main reason for this, despite the added mixing losses generated from the upstream blowing, was the reduction in losses associated with the passage vortex. Because the fan-shaped holes did not separate from the

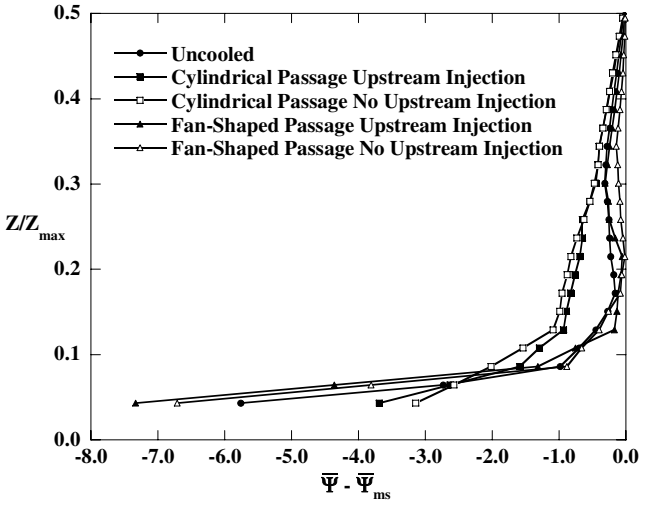

Fig. 7. Pitch-averaged exit flow angles for each flow field case.

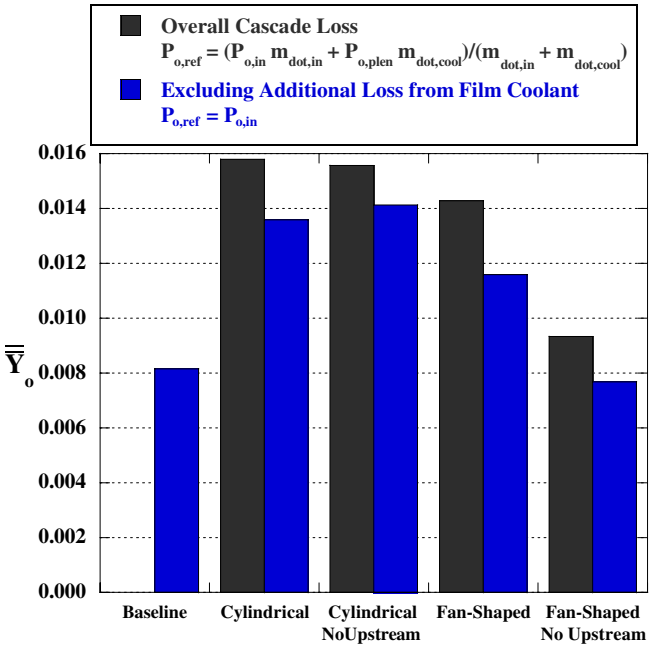

Fig. 8. Mass-averaged total pressure loss for each flow field case.

endwall surface as the cylindrical holes did, there was less interaction with the freestream and subsequently less mixing losses in the fan-shaped passage.

Using the inlet stagnation pressure as the reference stagnation pressure rather than Eq. (4) in the definition of the total pressure loss coefficient resulted in lower Y_0 values for each film-cooled case (shown in Fig. 8). The reason is that although Eq. (4) incorporated the additional energy being added to the passage flow by the coolant, it also included the losses that occur within the film-cooling holes.

The effect of upstream injection on the mass-averaged total pressure loss through the cascade depends on the

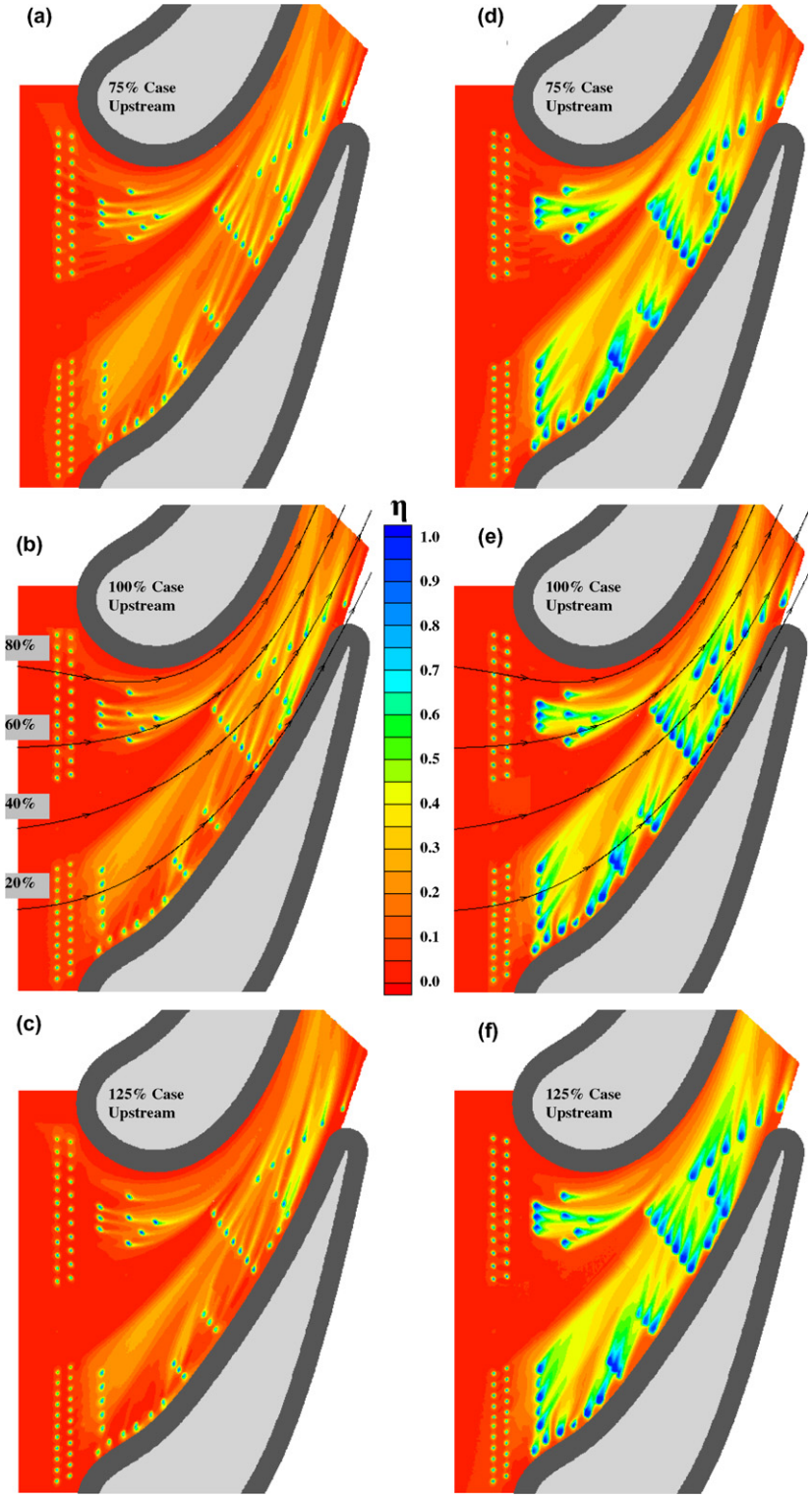

Fig. 9. Effectiveness contours with upstream coolant injection for the cylindrical (a–c) and fan-shaped passage (d–f).

film-cooling hole shape. With cylindrical holes, only a slight increase in $\overline{\overline{Y}}_0$ was seen. The reason was that the cylindrical holes in the passage separate and generate a large amount of mixing within the passage. Any additional mixing caused by the upstream blowing does not significantly add to the total pressure loss. The fan-shaped holes, on the other hand, do not separate and therefore do not generate large mixing losses by themselves. For this reason the mixing losses generated by the upstream blowing in the fan-shaped passage were much more significant in terms of raising the overall losses. The reduction in passage vortex losses for the fan-shaped passage also contributed to the

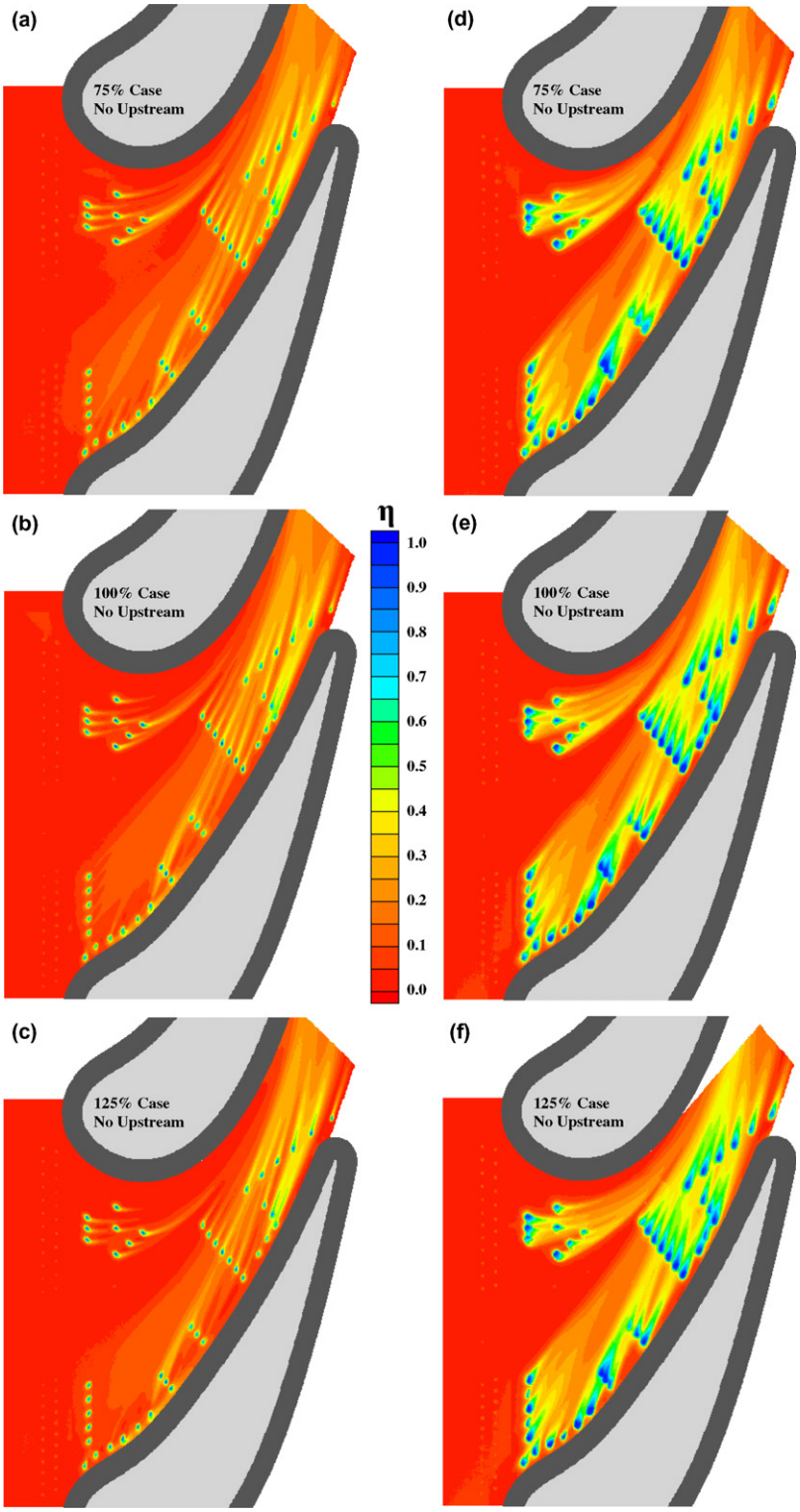

Fig. 10. Effectiveness contours without upstream coolant injection for the cylindrical (a–c) and fan-shaped passage (d–f).

lower mass-averaged $\overline{\overline{Y}}_0$ values than for the cylindrical passage. The study by Barigozzi et al. (2005) showed little difference between the losses generated for their fan-shaped passage versus their cylindrical passage. This however, was attributed to the different number of holes between the two passages. At the same mass flow rate, fewer holes in the fan-shaped passage caused higher jet velocities, leading to higher losses inside the hole than what would be seen if there had been a one-to-one comparison.

5. Thermal results

The following sections discuss the effect of upstream injection on the cooling performance of cylindrical and fan-shaped holes on a gas turbine endwall. Results are reported in terms of adiabatic film-cooling effectiveness, as defined by Eq. (6).

5.1. Adiabatic film-cooling effectiveness measurements

Adiabatic film-cooling effectiveness measurements are shown in Fig. 9(a)–(f) for the cases with upstream coolant injection and in Fig. 10(a)–(f) for the cases without upstream injection. The cases shown in Fig. 9(a)–(f) with upstream injection were described in detail by Colban et al. (2006a) and are shown in this paper for comparison purposes. It is particularly interesting that the upstream rows provided no immediate cooling benefit to the endwall surface in any of the contours in Fig. 9. All of the coolant ejected from the upstream holes was completely separated from the surface, even at the lowest tested flow rates due to the high surface angle.

In examining the differences between the cases without upstream coolant (shown in Fig. 10) and the cases with upstream coolant (shown in Fig. 9), it is immediately obvious that the overall levels of film-cooling effectiveness for the cases without upstream injection were much lower. This is interesting given the fact that the upstream holes offer no visible cooling benefit themselves, one would not expect levels further downstream to be greatly reduced in the absence of upstream injection, although certainly some of the improvement was probably due to a cooler near wall fluid from the upstream blowing. Pressure ratios were matched between cases shown in Figs. 9 and 10, so for instance, the passage film-cooling flow in Figs. 9(a) and 10(a) are directly comparable. In Figs. 10(a) and 9(a), the flow rate from the passage film-cooling holes was the same, the only difference being that the case in Fig. 9(a) had additional upstream coolant flow. Considering the fact that the amount of coolant issued from the film-cooling holes within the passage was the same for the cases in both Figs. 9 and 10, it is suggested and confirmed by the flowfield measurements that upstream coolant injection must alter the passage flow field in such a way as to make downstream endwall film-cooling more effective.

Fig. 11 shows the laterally averaged effectiveness in the cylindrical passage for the baseline case without upstream injection cooling. The general trend is increased $\bar{\eta}$ throughout the passage, indicating that film-cooling had a beneficial compounding effect. Also shown in Fig. 11 is the augmentation in laterally averaged film-cooling effectiveness for the 75% and 125% cases with respect to the baseline case. Just as for the case with upstream injection (Colban et al., 2006a), $\bar{\eta}$ decreased with increased coolant flow rate. The reason for this was that the cylindrical jets separated from the surface rendering inefficient endwall cooling, and the separation got worse with increasing coolant flow rate.

The laterally averaged film-cooling effectiveness and augmentation are shown for the fan-shaped passage with no upstream injection in Fig. 12. Again, $\bar{\eta}$ increased throughout the passage, with overall levels of $\bar{\eta}$ being much higher than the cylindrical passage without upstream injection (Fig. 11). The effect of increasing coolant flow rate on

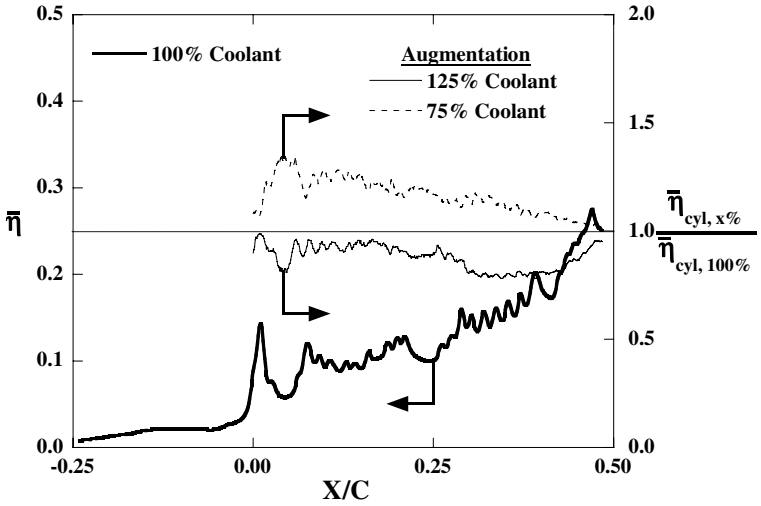

Fig. 11. Laterally averaged effectiveness for the 100% case and augmentation of laterally averaged effectiveness for the 75% and 125% cases on the cylindrical passage with no upstream cooling.

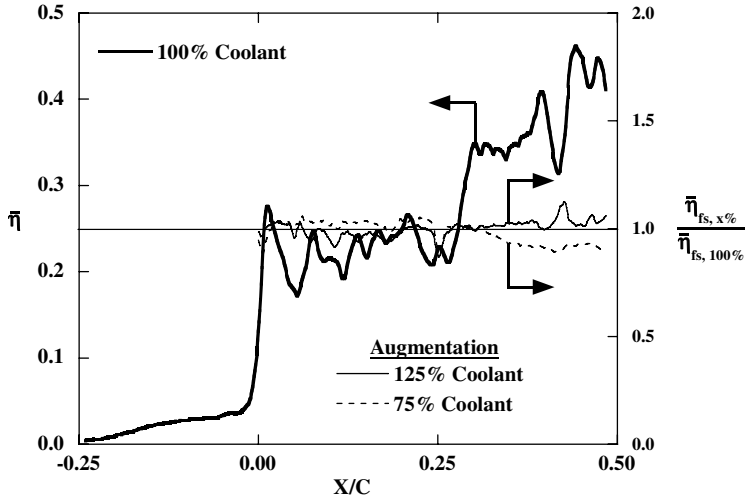

Fig. 12. Laterally averaged effectiveness for the 100% case and augmentation of laterally averaged effectiveness for the 75% and 125% cases on the fan-shaped passage with no upstream cooling.

the fan-shaped passage was opposite to the cylindrical passage. Because the fan-shaped holes diffused the coolant jet as it exited the hole, it was not prone to separation as was the cylindrical hole jet. For this reason, $\bar{\eta}$ increased with increasing coolant flow rate, yielding the intuitive result of increased cooling performance with increased coolant flow rate.

Figs. 13 and 14 both show the reduction in $\bar{\eta}$ without upstream coolant injection versus with upstream coolant injection. For both the cylindrical (Fig. 13) and the fan-shaped (Fig. 14) passage, it is clear that upstream coolant injection yielded a significant increase in $\bar{\eta}$. This effect was seen fairly uniformly across all measured coolant flow rates.

The augmentation in $\bar{\eta}$ for the fan-shaped passage versus the cylindrical passage without upstream coolant injection is shown in Fig. 15. Just as with upstream coolant injection (Colban et al., 2006a), the fan-shaped cooling holes offered

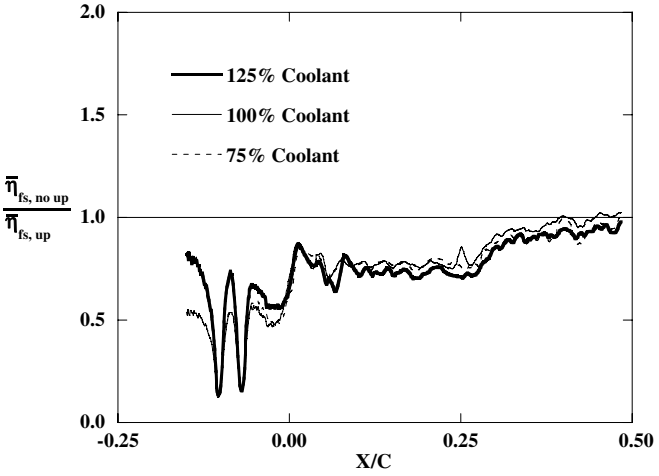

Fig. 14. Reduction of laterally-averaged film-cooling effectiveness for the fan-shaped passage with and without upstream cooling.

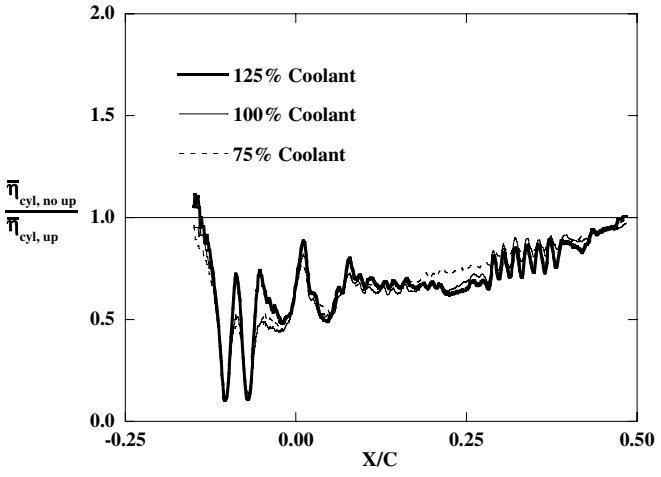

Fig. 13. Reduction of laterally-averaged film-cooling effectiveness for the cylindrical passage with and without upstream cooling.

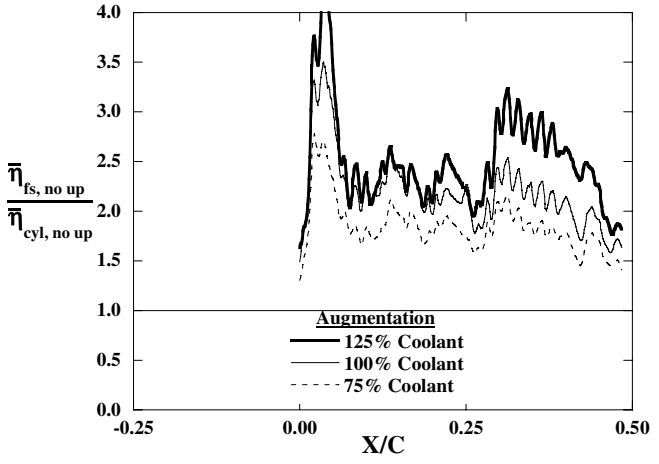

Fig. 15. Augmentation of laterally-averaged film-cooling effectiveness for fan-shaped cooling holes over cylindrical cooling holes without upstream injection.

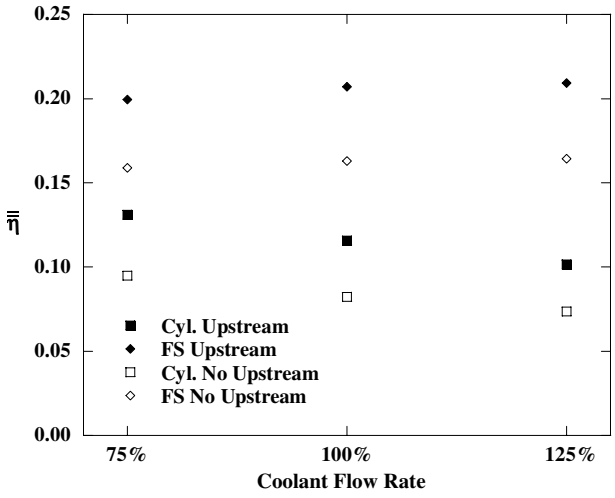

Fig. 16. Area-averaged film-cooling effectiveness for all cases.

significantly better film-cooling performance than their cylindrical counterparts. The augmentation in $\bar{\eta}$ increased with coolant flow rate as a result of the opposite influence of coolant flow rate on the $\bar{\eta}$ performance between the two passages.

5.2. Area-averaged film-cooling effectiveness

Area-averaged values of adiabatic film-cooling effectiveness were calculated over the endwall from $X/C = -0.25$ to $X/C = 0.5$ (the vane trailing edge) across one vane pitch. Area-averaged effectiveness offered a sense of the benefit gained by the entire endwall surface in any given cooling configuration (geometry and flow condition). Fig. 16 shows the area-averaged film-cooling effectiveness for each case reported in Table 3. Please note that the cases without upstream injection have less total coolant than the cases with upstream injection. The trends of increasing effectiveness with coolant flow rate for the fan-shaped passage, and decreasing effectiveness with coolant flow rate for the cylindrical passage can be seen clearly. The trend between the cases with and without upstream coolant injection was not linear (although not shown clearly on this graph because the actual coolant flow rates were proprietary), which suggests that the upstream coolant injection altered the flowfield in such a way as to allow the downstream film-cooling to be more effective.

6. Conclusions

As mentioned previously, the goals of this study were to evaluate the aerodynamic and cooling performance of cylindrical and fan-shaped holes on an endwall for a turbine airfoil. Although there is no conventional parameter that combines both cooling benefits and aerodynamic losses into one overall performance metric, the work presented in this paper evaluated each through the analysis of experimental data. A five-hole total pressure probe was used to measure the exit plane flowfield with and without upstream injection for passages featuring cylindrical and fan-shaped holes. An infrared camera was used to measure adiabatic film-cooling effectiveness for both fan-shaped and cylindrical passages with and without upstream injection.

Cylindrical hole film-cooling increased the total pressure losses generated by the passage vortex. Cylindrical hole film-cooling did reduce the strength of the cross-passage flow, shifting the location of the passage vortex towards the pressure side. The coolant separation in the cylindrical passage, which was evident from the effectiveness contours, generated high mixing losses with the freestream. The fan-shaped holes did not separate from the endwall, but the shear layer between the coolant and the freestream still generated significant losses.

Both passages showed increased mixing and shear losses with upstream injection relative to no upstream injection. Overall mass-averaged losses for the cylindrical passage were much higher than the uncooled case because of the increase in passage vortex losses and the added mixing losses. Overall mass-averaged losses for the fan-shaped passage were nearly the same as for the uncooled case because the added shear layer losses were counteracted by the reduction in losses generated by the passage vortex. The flowfield results showed that fan-shaped holes generated less total pressure loss than cylindrical holes, especially with no upstream blowing.

The adiabatic film-cooling effectiveness measurements showed that the coolant from the upstream holes had little immediate cooling benefit to the endwall in the region just downstream of the upstream injection, with the coolant separating entirely from the endwall because of the high injection angle. However, further downstream in the passage, effectiveness levels for the cases with upstream coolant were much higher, the reason being that there was a large amount of coolant in the passage region from the upstream injection. This coolant mixed with the freestream and lowered the temperature of the near-wall fluid, resulting in higher effectiveness levels downstream in the passage. The flow field results also indicated an influence on the passage flowfield by the upstream coolant injection, which could have also contributed to the higher effectiveness levels. The effect of increased coolant flow rate was to decrease $\bar{\eta}$ in the cylindrical passage because of jet separation. In the fan-shaped passage the effect of increased coolant flow rate was to increase $\bar{\eta}$ because the fan-shaped coolant jets stayed attached to the surface.

The results of this study further illustrate the complexity of the film-cooling design process. The addition of film-cooling holes on a turbine endwall has aerodynamic consequences in addition to the thermal benefit that might be gained. Incorrect placement of film-cooling holes can also prove wasteful. It is critical that engine designers be aware of both the thermal and aerodynamic consequences of their film-cooling hole designs. The results of this study are clear in their recommendation of fan-shaped holes over

cylindrical holes from both an aerodynamic and thermal perspective. Fan-shaped holes performed better aerodynamically than cylindrical holes, generating fewer total pressure losses through the turbine cascade. Fan-shaped holes also offered better cooling than cylindrical, both with and without upstream injection. Clearly, from an overall performance standpoint, fan-shaped holes were the superior cooling hole geometry.

Acknowledgments

The authors are grateful to Siemens Power Generation for their funding and support of this project and Mr. Michael Haendler for providing his guidance.

References

Barigozzi, G., Benzoni, G., Franchini, G., Perdichizzi, A., 2005. Fan-shaped hole effects on the aero-thermal performance of a film cooled endwall, ASME GT2005-68544.

Becz, S., Majewski, M.S., Langston, L.S., 2003. Leading edge modification effects on turbine cascade endwall loss, ASME GT2003-38898.

Blair, M.F., 1974. An experimental study of heat transfer and film cooling on large-scale turbine endwalls. ASME J. Heat Transfer 96, 524–529.

Bogard, D.G., Thole, K.A., 2006. Gas turbine film cooling. AIAA J. Prop. Pow. 22, 249–270.

Bunker, R.S., 2005. A review of shaped hole turbine film-cooling technology. ASME J. Heat Transfer 127, 441–453.

Colban, W., Thole, K.A., Zess, G., 2003. Combustor turbine interface studies – Part 1: Endwall effectiveness measurements. ASME J. Turbo. 125, 193–202.

Colban, W., Thole, K.A., Haendler, M., 2005. Experimental and computational comparisons of fan-shaped film-cooling on a turbine vane surface, ASME IMECE2005-79596.

Colban, W., Thole, K.A., Haendler, M., 2006a. A comparison of cylindrical and fan-shaped film-cooling holes on a vane endwall at low and high freestream turbulence levels, ASME GT2006-90021.

Colban, W., Gratton, A., Thole, K.A., Haendler, M., 2006b. Heat transfer and film-cooling measurements on a stator vane with fan-shaped cooling holes. ASME J. Turbo. 128, 53–61.

Friedrichs, S., Hodson, H.P., Dawes, W.N., 1995. Distribution of film-cooling effectiveness on a turbine endwall measured using the ammonia and diazo technique. ASME J. Turbo. 118, 613–621.

Friedrichs, S., Hodson, H.P., Dawes, W.N., 1997. Aerodynamic aspects of endwall film-cooling. ASME J. Turbo. 119, 786–793.

Goldstein, R.J., 1971. Film cooling. Adv. Heat Transfer 7, 321–379.

Granser, D., Schulenberg, T., 1990. Prediction and measurement of film cooling effectiveness for a first stage turbine vane shroud, ASME 90-GT-95.

Harasgama, S.P., Burton, C.D., 1992. Film cooling research on the endwall of a turbine nozzle guide vane in a short duration annular cascade: Part 1 – Experimental technique and results. ASME J. Turbo. 114, 734–740.

Kercher, D.M., 2003. Film-cooling bibliography: 1940–2002, Private publication.

Kercher, D.M., 2005. Film-cooling bibliography addendum: 1999–2004, Private publication.

Knost, D.G., Thole, K.A., 2003. Computational predictions of endwall film-cooling for a first stage vane, ASME GT2003-38252.

Knost, D.G., Thole, K.A., 2005. Adiabatic effectiveness measurements of endwall film-cooling for a first stage vane. ASME J. Turbo. 127, 297–305.

Kost, F., Nicklas, M., 2001. Film-cooled turbine endwall in a transonic flow field: Part I – Aerodynamic measurements, ASME 2001-GT-0145.

Langstion, L.S., 1980. Crossflows in a turbine cascade passage. ASME J. Eng. Pow. 102, 866–874.

Langston, L.S., Nice, M.L., Hooper, R.M., 1977. Three-dimensional flow within a turbine cascade passage. ASME J. Eng. Pow. 99, 21–28.

Lethander, A.T., Thole, K.A., 2003. Optimizing the vane-endwall junction to reduce adiabatic wall temperatures in a turbine vane passage, ASME GT2003-38940.

Mahmood, G.I., Gustafson, R., Acharya, S., 2005. Experimental investigation of flow structure and Nusselt number in a low-speed linear blade passage with and without leading-edge fillets. ASME J. Heat Transfer 127, 499–512.

Moffat, R.J., 1988. Describing the uncertainties in experimental results. Exp. Therm. Fluid Sci. 1, 3–17.

Nicklas, M., 2001. Film-cooled turbine endwall in a transonic flow field: Part II – Heat transfer and film-cooling effectiveness, ASME 2001-GT-0146.

Oke, R.A., Burd, S.W., Simon, T.W., Vahlberg, R., 2000. Measurements in a turbine cascade over a contoured endwall: discrete hole injection of bleed flow, ASME 2000-GT-214.

Sieverding, C.H., Wilputte, P., 1981. Influence of mach number and endwall cooling on secondary flows in a straight nozzle cascade. ASME J. Eng. Gas Turb. Pow. 103, 257–264.

Zess, G., Thole, K.A., 2002. Computational design and experimental evaluation of using a leading edge fillet on a gas turbine engine. ASME J. Turbo. 124, 167–175.

Zhang, L.J., Jaiswal, R.S., 2001. Turbine nozzle endwall film cooling study using pressure-sensitive paint. ASME J. Turbo. 123, 730–738.

Zhang, L., Moon, H.K., 2003. Turbine nozzle endwall inlet film cooling – the effect of a back-facing step, ASME GT2003-38319.